Numerical results using a colocated finite-volume scheme on unstructured grids for incompressible fluid flows

Eric Chénier, R. Eymard, O. Touazi

Numerical results using a colocated finite volume scheme on unstructured grids for incompressible fluid flows

E. Chénier, R. Eymard, O. Touazi*
LETEM, Université de Marne-la-Vallée, Bât. Lavoisier, 77454 Marne-la-Vallée Cedex, France

Abstract

This paper presents numerical results, using a new finite volume scheme on unstructured grids for the incompressible Navier-Stokes equations. The discrete unknowns are the components of the velocity, the pressure and the temperature, colocated at the centers of the control volumes. The scheme is stabilized, using an original method leading to local redistributions of the fluid mass, which simultaneously yields the control of the kinetic energy and the convergence of the scheme. Different comparisons with the literature (2D and 3D lid driven cavity, backward facing step, differentially heated cavity) allow to assess the numerical properties of the scheme.

1 Introduction

The problem of finding approximate solutions for the incompressible Navier-Stokes equations has been extensively studied and numerous schemes have already been presented in the literature (see the review article [1] and the important numerical works concerning the finite element methods [2, 3, 4, 5] and references therein).

In the engineering framework, finite volume schemes have been widely used on Cartesian grids or orthogonal meshes, following the pioneering works of [6]. Historically, unstructured grid solvers have been mainly developed in the framework of density-based numerical method for compressible flows. Most of the numerical developments of finite volume schemes for incompressible flows have been performed on structured grids in the spirit of the classical Marker And Cell scheme (MAC), formulated originally by Harlow and Welch [7]. Amongst the attempts to extend the MAC-scheme to unstructured meshes, Nicolaides [8] proposed the "dual mesh" or "covolume" method taking advantage of the fact that an unstructured tetrahedral mesh, under the Delaunay condition, can be associated to a Voronoï tessellation. However, most of the grid solvers so obtained are of low order accuracy due to reconstructions from staggered data : these methods tend to be first order accurate on nonuniform meshes. Some numerical improvements had been proposed to increase the convergence speed [9]. Note also some recent mathematical works on the convergence of a finite volume scheme for unstructured staggered grids (see [10, 11] for the Stokes problem and [12] for the Navier-Stokes equations).

* *E-mail address:* touazi@univ-mlv.fr

An obvious alternative of using staggered meshes is to express all the variables on the same grid. This method has become popular for pressure-based solvers since the work of Rhie and Chow [13]. For instance, Mathur and Murthy [14, 15] proposed a colocated SIMPLE-based solver with a dissipation term in the mass equation to avoid spurious oscillations on pressure modes. The gradients on faces are however not easy to define and give rise to several expressions according to the authors [14], [15], [16]; an inconsistent gradient expression may lead to a residual error on the diffusion fluxes within grid refinement. Therefore Perron *et al.* [17] have proposed a novel approach where variables are located at cell-circumcenters, the time discretization being based upon the fractional time step method [18]. The decoupling method allowed by this time discretization leads to compute an intermediate normal velocity on faces, which prevents from the classical spurious pressure oscillations. On the contrary, a coupled stabilization strategy, which leads to a global matter redistribution, has been applied to a colocated finite element method for the steady linear Stokes problem [19].

Using some of these ideas, we present here an original colocated finite volume scheme to solve the Navier-Stokes equations in the framework of incompressible flows on structured or unstructured grids, focusing both on numerical implementation and comparisons to benchmark solutions (the mathematical proof of convergence of the scheme is detailed in [20]). The key points of this scheme are the following:

1. the unknowns are colocated at some particular points, called centers of the control volumes;

2. the only requirement for the finite volume grids is that each interface between two adjacent control volumes is orthogonal to the line joining their centers;

3. the discrete gradient of the pressure and the discrete divergence of the velocity are dual operators, and the nonlinear convective term in the momentum equation is discretized so that the discrete kinetic energy is time decreasing;

4. a stabilization term is introduced in the mass equation, leading only to a local redistribution of the matter, thus preserving the global convergence;

5. the set of discrete equations is simultaneously solved by an under-relaxed Newton's method with a direct or an iterative linear solver (in this paper, the BICGSTAB method is used).

The outlines of this paper are the following. In Section 2 are presented the numerical scheme and the main features of its practical implementation. In Section 3, 2D and 3D numerical examples are provided for either isothermal flows or natural thermal convection. Conclusions are then drawn in Section 4.

2 Numerical method

We consider the incompressible fluid flow under the Boussinesq approximation in a 2D or 3D space domain, denoted by Ω, the time variable varying between 0 and T. The mass,

momentum and energy equations are

$$\begin{aligned} \vec{\nabla}.\vec{v} &= 0, \\ \frac{\partial}{\partial t}\vec{v} + \vec{\nabla}.(\vec{v}\otimes\vec{v}) + \frac{1}{\rho}\vec{\nabla}p - \nu\Delta\vec{v} &= \vec{f}(T), \\ \frac{\partial}{\partial t}T + \vec{\nabla}.(\vec{v}T) - \alpha\Delta T &= s, \end{aligned}$$

where $\vec{v}(x,t)$ is the velocity field, $p(x,t)$ is the pressure field, $T(x,t)$ is the temperature field, ν is the kinematic viscosity, α is the thermal diffusivity, ρ is the density and $\vec{f}$ and s are source terms such as buoyant forces and heat source or sink. In addition to the conservative equations, initial (at $t = 0$) and boundary (on $\partial\Omega$) conditions are imposed. At last, we suppose that the domain Ω is completely recovered by a family $\mathcal{M}$ of control volumes. We now introduce convenient notations which are summarized in Figure 1 in the 2D-case:

- for all control volume K ($K \in \mathcal{M}$), we denote by $\mathcal{E}_K$ the set of its edges and by $\mathcal{E}_{K,\text{ext}}$ the subset of its edges located at the boundary $\partial\Omega$;
- for all control volume K ($K \in \mathcal{M}$), we denote by m_K its area (if $d = 2$) or its volume (if $d = 3$) and by X_K its "center";
- for all control volume K ($K \in \mathcal{M}$), we denote by $\mathcal{N}_K$ the set composed by the neighbors of K;
- for any neighboring control volume L of K ($L \in \mathcal{N}_K$), we denote by σ_{KL} its common edge, assuming that the straight line (X_K, X_L) is orthogonal to σ_{KL};
- for any neighboring control volume L of K ($L \in \mathcal{N}_K$), we denote by m_{KL} the interface length ($d = 2$) or area ($d = 3$) between K and L, by $\vec{n}_{KL}$ the unit vector, normal to σ_{KL} and oriented from K to L and by d_{KL} the distance between X_K and X_L;
- for each edge σ located at the boundary domain ($\sigma \in \mathcal{E}_{K,\text{ext}}$), we denote by X_σ the orthogonal projection of X_K on σ, by $\vec{n}_{K,\sigma}$ the unit vector normal to σ outward K and by $d_{K,\sigma}$ the distance between X_K and X_σ.

Finite volume meshes which meet the above geometrical requirements can easily be found:

- rectangular grids ($d = 2$) or right parallelepipedic ($d = 3$) grids are the simplest examples,
- triangular grids ($d = 2$) with acute angles are convenient (the center X_K is that of the circumcircle),
- Voronoï tesselations ($d = 2$ and $d = 3$) offer very powerful grid possibilities. Recall that the control volume K is defined in this case as the set of points closer to X_K than to any other X_L: the interfaces are then included in the midhyperplanes between centers X_K and X_L, thus ensuring by construction the required orthogonality property. Two important advantages can be drawn from the use of such meshes. First, grid refinement strategies can easily be designed within the knowledge of an a posteriori error estimate. Indeed, a refinement procedure of such a mesh consists in the introduction of new points,

which only lead to a local modification of the mesh. Secondly, this method allows for meshing any 2D and 3D domains, whatever the complexity of their geometry, the nature of their boundaries (curved or planar). Note that powerful tools for the generation of Voronoï tesselations are available on the web.

The time interval $[0,T]$ is discretized by $t^0 = 0 < t^1 < \ldots < t^n < t^{n+1} < \ldots < t^N = T$.

The scheme consists in computing, at each time step $n = 0, \ldots, N-1$ and for all $K \in \mathcal{M}$, approximation values $\vec{v}_K^{n+1}$, p_K^{n+1} and T_K^{n+1} of the continuous unknowns expressed at the center cell X_K and at time t^n, $\vec{v}(X_K, t^{n+1})$, $p(X_K, t^{n+1})$ and $T(X_K, t^{n+1})$. These discrete unknowns are solutions of algebraic relations which are from now on explained in details.

2.1 Scheme for unsteady problems

For all $n = 0, \ldots, N-1$, the conservative equations are expressed in time with a second order centered scheme, namely the Cranck-Nicholson scheme, where the unknowns are the discrete fields $\vec{v}^{n+1}$, $p^{n+1/2}$ and T^{n+1}:

$$\begin{aligned} \vec{\nabla}.\vec{v}^{n+1/2} &= 0 \\ \frac{\vec{v}^{n+1}-\vec{v}^{n}}{t^{n+1}-t^{n}} + \vec{\nabla}.\left(\vec{v}^{n+1/2}\otimes\vec{v}^{n+1/2}\right) + \frac{1}{\rho}\vec{\nabla}p^{n+1/2} - \nu\Delta\vec{v}^{n+1/2} &= \vec{f}(T^{n+1/2}) \\ \frac{T^{n+1}-T^{n}}{t^{n+1}-t^{n}} + \vec{\nabla}.\left(\vec{v}^{n+1/2}T^{n+1/2}\right) - \alpha\Delta T^{n+1/2} &= s^{n+1/2} \end{aligned}$$

with $\vec{v}^{n+1/2} = 0.5 \times (\vec{v}^{n} + \vec{v}^{n+1})$, $T^{n+1/2} = 0.5 \times (T^{n} + T^{n+1})$. For convenience, the equations are rewritten using only the unknowns $\vec{v}^{n+1/2}$, $p^{n+1/2}$ and $T^{n+1/2}$:

$$\vec{\nabla}\cdot\vec{v}^{n+1/2} = 0 \quad (1)$$

$$2\frac{\vec{v}^{n+1/2}-\vec{v}^{n}}{t^{n+1}-t^{n}} + \vec{\nabla}\cdot\left(\vec{v}^{n+1/2}\otimes\vec{v}^{n+1/2}\right) + \frac{1}{\rho}\vec{\nabla}p^{n+1/2} - \nu\Delta\vec{v}^{n+1/2} = \vec{f}(T^{n+1/2}) \quad (2)$$

$$2\frac{T^{n+1/2}-T^{n}}{t^{n+1}-t^{n}} + \vec{\nabla}\cdot\left(\vec{v}^{n+1/2}T^{n+1/2}\right) - \alpha\Delta T^{n+1/2} = s^{n+1/2} \quad (3)$$

The spatial discretization is based on the finite volume method. The continuous equations (1-3) are integrated in any control volume $K \in \mathcal{M}$ and Green's formula is applied:

- Mass equation

$$\sum_{L\in\mathcal{N}_K} \mathcal{F}_{KL}(\vec{v}^{n+1/2}) + \sum_{\sigma\in\mathcal{E}_{K,\text{ext}}} \mathcal{F}_{K,\sigma}(\vec{v}^{n+1/2}) = 0$$

with

$$\begin{cases} \mathcal{F}_{KL}(\vec{v}) = \displaystyle\int_{\sigma_{KL}} \vec{v}(x)\cdot\vec{n}_{KL}\,\mathrm{ds(x)} \\ \mathcal{F}_{K,\sigma} = \displaystyle\int_{\sigma} \overline{\vec{v}}(x)\cdot\vec{n}_{K,\sigma}\,\mathrm{ds}(x) \end{cases}$$

- momentum equation

$$\frac{2}{t^{n+1}-t^n}\left(\int_K \vec{v}^{n+1/2}(x)\,\mathrm{d}x - \int_K \vec{v}^{n}(x)\mathrm{d}(x)\right) + \sum_{L\in\mathcal{N}_K} \vec{\mathcal{G}}_{KL}(\vec{v}^{n+1/2},p^{n+1/2}) + \sum_{\sigma\in\mathcal{E}_{K,\mathrm{ext}}} \vec{\mathcal{G}}_{K,\sigma}(\vec{v}^{n+1/2},p^{n+1/2}) = \int_K \vec{f}(T^{n+1/2}(x))\,\mathrm{d}x,$$

with

$$\begin{cases} \vec{\mathcal{G}}_{KL}(\vec{v},p) = \displaystyle\int_{\sigma_{KL}} \left((\vec{v}(x)\cdot\vec{n}_{KL})\vec{v}(x) + \frac{1}{\rho}p(x)\vec{n}_{KL} - \nu\vec{\nabla}\vec{v}(x)\cdot\vec{n}_{KL}\right)\mathrm{ds}(x) \\ \vec{\mathcal{G}}_{K,\sigma}(\vec{v},p) = \displaystyle\int_{\sigma} \left(\vec{v}(x)\cdot\vec{n}_{K,\sigma}\vec{v}(x) + \frac{1}{\rho}p(x)\vec{n}_{K,\sigma} - \nu\vec{\nabla}\vec{v}(x)\cdot\vec{n}_{K,\sigma}\right)\mathrm{ds}(x) \end{cases}$$

- energy equation

$$\frac{2}{t^{n+1}-t^n}\left(\int_K T^{n+1/2}(x)\,\mathrm{d}x - \int_K T^{n}(x)\,\mathrm{d}x\right) + \sum_{L\in\mathcal{N}_K} \mathcal{H}_{KL}(\vec{v}^{n+1/2},T^{n+1/2}) + \sum_{\sigma\in\mathcal{E}_{K,\mathrm{ext}}} \mathcal{H}_{K,\sigma}(\vec{v}^{n+1/2},T^{n+1/2}) = \int_K s^{n+1/2}(x)\,\mathrm{d}x,$$

with

$$\begin{cases} \mathcal{H}_{KL}(\vec{v},T) = \displaystyle\int_{\sigma_{KL}} \left((\vec{v}(x)\cdot\vec{n}_{KL})T(x) - \alpha\vec{\nabla}T(x)\cdot\vec{n}_{KL}\right)\mathrm{ds}(x) \\ \mathcal{H}_{K,\sigma}(\vec{v},T) = \displaystyle\int_{\sigma} \left((\vec{v}(x)\cdot\vec{n}_{K,\sigma})T(x) - \alpha\vec{\nabla}T(x)\cdot\vec{n}_{K,\sigma}\right)\mathrm{ds}(x) \end{cases}$$

The integrals $\mathcal{F}_{KL}(\vec{v})$, $\mathcal{F}_{K,\sigma}$, $\vec{\mathcal{G}}_{KL}(\vec{v},p)$, $\vec{\mathcal{G}}_{K,\sigma}(\vec{v},p)$, $\mathcal{H}_{KL}(\vec{v},T)$ and $\mathcal{H}_{K,\sigma}(\vec{v},T)$ are approximated by the following centered expressions:

$$\begin{array}{lcl} F_{KL}(\vec{v}_K,\vec{v}_L,p_K,p_L) & = & m_{KL}\frac{\vec{v}_K+\vec{v}_L}{2}\cdot\vec{n}_{KL} - \lambda_{KL}\frac{m_{KL}}{d_{KL}}(p_L-p_K), \\ F_{K,\sigma} & = & m_\sigma\overline{\vec{v}}_\sigma\cdot\vec{n}_{K,\sigma} \\ \vec{G}_{KL}(\vec{v}_K,\vec{v}_L,p_K,p_L) & = & F_{KL}(\vec{v}_K,\vec{v}_L,p_K,p_L)\frac{\vec{v}_K+\vec{v}_L}{2} + \frac{1}{\rho}m_{KL}\frac{p_L+p_K}{2}\vec{n}_{KL} \\ & & -\nu\frac{m_{KL}}{d_{KL}}(\vec{v}_L-\vec{v}_K) \\ \vec{G}_{K,\sigma}(\vec{v}_K,p_K) & = & F_{K,\sigma}\vec{v}_K + \frac{1}{\rho}m_\sigma p_K\vec{n}_{K,\sigma} - \nu\frac{m_\sigma}{d_{K,\sigma}}(\overline{\vec{v}}_\sigma-\vec{v}_K) \\ H_{KL}(\vec{v}_K,\vec{v}_L,p_K,p_L,T_K,T_L) & = & F_{KL}(\vec{v}_K,\vec{v}_L,p_K,p_L)\frac{T_K+T_L}{2} - \alpha\frac{m_{KL}}{d_{KL}}(T_L-T_K) \\ H_{K,\sigma}(\vec{v}_K,p_K,T_K) & = & F_{K,\sigma}T_K - \alpha\frac{m_\sigma}{d_{K,\sigma}}(\overline{T}_\sigma - T_K). \end{array}$$

with λ_{KL} being a stabilization parameter defined on each interface between two control volumes K and L which will be discussed in Subsection 2.5.

Consequently, the scheme for transient problems writes:

$$\begin{array}{lcl} \displaystyle\sum_{L\in\mathcal{N}_K} F_{KL}(\vec{v}_K,\vec{v}_L,p_K,p_L)^{n+1/2} + \sum_{\sigma\in\mathcal{E}_{K,\mathrm{ext}}} F_{K,\sigma}^{n+1/2} & = & 0 \\ \frac{2\ m_K}{t^{n+1}-t^n}(\vec{v}_K^{n+1/2}-\vec{v}_K^{n})+ & & \\ \displaystyle\sum_{L\in\mathcal{N}_K} \vec{G}_{KL}(\vec{v}_K,\vec{v}_L,p_K,p_L)^{n+1/2} + \sum_{\sigma\in\mathcal{E}_{K,\mathrm{ext}}} \vec{G}_{K,\sigma}(\vec{v}_K,p_K)^{n+1/2} & = & m_K\vec{f}(T_K^{n+1/2}) \\ \frac{2\ m_K}{t^{n+1}-t^n}(T_K^{n+1/2}-T_K^{n})+ & & \\ \displaystyle\sum_{L\in\mathcal{N}_K} H_{KL}(\vec{v}_K,\vec{v}_L,p_K,p_L,T_K,T_L)^{n+1/2} + \sum_{\sigma\in\mathcal{E}_{K,\mathrm{ext}}} H_{K,\sigma}(\vec{v}_K,T_K)^{n+1/2} & = & m_K s_K^{n+1/2} \end{array} \qquad (4)$$

Hence the finite volume scheme is completely determined under the knowledge of the position of the edges and of the centers of the control volumes. The computing time needed for preparing the data before finding an approximate solution appears to be negligible in practice.

2.2 Properties of the scheme

For a given time step index n, we denote by $\vec{v}_\mathcal{M}$, $p_\mathcal{M}$ and $T_\mathcal{M}$ the piecewise constant functions respectively defined by the values $\vec{v}_K^{n+1/2}$, $p_K^{n+1/2}$ and $T_K^{n+1/2}$ for all x in K. Defining the discrete gradient operator $\vec{\nabla}_\mathcal{M}$ by

$$m_K(\vec{\nabla}_\mathcal{M} p_\mathcal{M})_K = \sum_{L\in\mathcal{N}_K} m_{KL}\frac{p_L^{n+1/2}+p_K^{n+1/2}}{2}\vec{n}_{KL} + \sum_{\sigma\in\mathcal{E}_{K,\text{ext}}} m_\sigma p_K^{n+1/2}\vec{n}_{K,\sigma},$$

the relation $\sum_{L\in\mathcal{N}_K} m_{KL}\vec{n}_{KL} + \sum_{\sigma\in\mathcal{E}_{K,\text{ext}}} m_\sigma \vec{n}_{K,\sigma} = \vec{0}$ leads to

$$m_K(\vec{\nabla}_\mathcal{M} p_\mathcal{M})_K = \sum_{L\in\mathcal{N}_K} m_{KL}\frac{p_L^{n+1/2}-p_K^{n+1/2}}{2}\vec{n}_{KL},$$

which shows that the discrete gradient operator $\vec{\nabla}_\mathcal{M}$ is the dual of the discrete divergence operator $\vec{\nabla}_\mathcal{M}\cdot$ defined by

$$m_K(\vec{\nabla}_\mathcal{M}\cdot\vec{v}_\mathcal{M})_K = \sum_{L\in\mathcal{N}_K} m_{KL}\frac{\vec{v}_K^{n+1/2}+\vec{v}_L^{n+1/2}}{2}\cdot\vec{n}_{KL},$$

in the sense that it meets the property

$$\int_\Omega \vec{\nabla}_\mathcal{M} p_\mathcal{M}(x)\cdot\vec{v}_\mathcal{M}(x)\,\mathrm{d}x = -\int_\Omega p_\mathcal{M}(x)\vec{\nabla}_\mathcal{M}\cdot\vec{v}_\mathcal{M}(x)\,\mathrm{d}x.$$

We can then prove an important consequence (which cannot be drawn from schemes where this dual property is not satisfied): the scheme (4) prevents from the increase of the discrete kinetic energy. Indeed, let us assume that the boundary conditions are such that $\overline{\vec{v}}_\sigma = \vec{0}$ and $\vec{f} = 0$. We then multiply the discrete momentum balance by $\vec{v}_K^{n+1/2}$ and sum over $K\in\mathcal{M}$. Thanks to the dual property of the discrete operators and to the discrete conservation of the fluid mass (which makes the nonlinear terms vanish; such a property is only obtained for constant space steps on the MAC scheme), we thus obtain

$$\begin{aligned}
&\frac{1}{t^{n+1}-t^n}\sum_{K\in\mathcal{M}} m_K\left(\frac{(\vec{v}_K^{n+1})^2}{2}-\frac{(\vec{v}_K^{n})^2}{2}\right)\\
&+\sum_{\sigma=\sigma_{KL}}\frac{m_{KL}}{d_{KL}}\left(\nu\,(\vec{v}_L^{n+1/2}-\vec{v}_K^{n+1/2})^2+\lambda_{KL}(p_L^{n+1/2}-p_K^{n+1/2})^2\right)\\
&+\sum_{K\in\mathcal{M}}\sum_{\sigma\in\mathcal{E}_{K,\text{ext}}}\frac{m_\sigma}{d_{K,\sigma}}\nu\,(\vec{v}_K^{n+1/2})^2 \qquad\qquad = 0,
\end{aligned}$$

and prove the following kinetic energy inequality

$$\begin{aligned}
&\sum_{K\in\mathcal{M}} m_K\frac{(\vec{v}_K^{n+1})^2}{2}+\\
&(t^{n+1}-t^n)\left(\sum_{\sigma=\sigma_{KL}}\frac{m_{KL}}{d_{KL}}\nu\,(\vec{v}_L^{n+1/2}-\vec{v}_K^{n+1/2})^2+\sum_{K\in\mathcal{M}}\sum_{\sigma\in\mathcal{E}_{K,\text{ext}}}\frac{m_\sigma}{d_{K,\sigma}}\nu\,(\vec{v}_K^{n+1/2})^2\right)\le\sum_{K\in\mathcal{M}} m_K\frac{(\vec{v}_K^{n})^2}{2}.
\end{aligned}$$

2.3 Upstream weighting version of the scheme

For a too large grid size, the local Reynolds number, $\frac{|\frac{1}{2}(\vec{v}_K+\vec{v}_L)\cdot\vec{n}_{KL}|d_{KL}}{\nu}$, or Péclet number, $\frac{|\frac{1}{2}(\vec{v}_K+\vec{v}_L)\cdot\vec{n}_{KL}|d_{KL}}{\alpha}$, can greatly exceed 1 at the interface between neighboring control volumes K and L. In such a case and to keep the scheme stable, it can be useful to substitute in the approximated transport terms, the centered expression $F_{KL}(\vec{v}_K,\vec{v}_L,p_K,p_L)\frac{\vec{v}_K+\vec{v}_L}{2}$ or $F_{KL}(\vec{v}_K,\vec{v}_L,p_K,p_L)\frac{T_K+T_L}{2}$ by the corresponding upstream weighting expressions given by

$\max(F_{KL}(\vec{v}_K,\vec{v}_L,p_K,p_L),0)\vec{v}_K + \min(F_{KL}(\vec{v}_K,\vec{v}_L,p_K,p_L),0)\vec{v}_L$, or

$\max(F_{KL}(\vec{v}_K,\vec{v}_L,p_K,p_L),0)T_K + \min(F_{KL}(\vec{v}_K,\vec{v}_L,p_K,p_L),0)T_L$.

It is also possible to introduce local upstream weights which depend on the local Reynolds or Péclet numbers. We do not present examples of the use of such a scheme in this paper, since we focus in the numerical examples on the precision of the results. Therefore we use sufficiently fine grids, choosing the size of the mesh h such that $\frac{\|\vec{v}\|h}{\nu}$ and $\frac{\|\vec{v}\|h}{\alpha}$, are small enough, according to an average norm of the velocity $\|\vec{v}\|$.

2.4 Scheme for the steady problem

The steady scheme is directly deduced from (4). The relations for determining discrete values for the steady unknowns $\vec{v}_K$, p_K, T_K, for $K\in\mathcal{M}$ are given by:

$$\left|\begin{array}{rcl}
\displaystyle\sum_{L\in\mathcal{N}_K} F_{KL}(\vec{v}_K,\vec{v}_L,p_K,p_L) + \sum_{\sigma\in\mathcal{E}_{K,\text{ext}}} F_{K,\sigma} & = & 0 \\
\displaystyle\sum_{L\in\mathcal{N}_K} \vec{G}_{KL}(\vec{v}_K,\vec{v}_L,p_K,p_L) + \sum_{\sigma\in\mathcal{E}_{K,\text{ext}}} \vec{G}_{K,\sigma}(\vec{v}_K,p_K) & = & m_K\vec{f}(T_K) \\
\displaystyle\sum_{L\in\mathcal{N}_K} H_{KL}(\vec{v}_K,\vec{v}_L,p_K,p_L,T_K,T_L) + \sum_{\sigma\in\mathcal{E}_{K,\text{ext}}} H_{K,\sigma}(\vec{v}_K,T_K) & = & m_K s_K
\end{array}\right. \tag{5}$$

2.5 The stabilization method and the parameter λ_{KL}

It is well known that a stabilization method is necessary to prevent from the apparition of oscillations in colocated schemes since, intuitively speaking, the number of pressure unknowns is too large compared to that of velocity unknowns. This problem has been handled in the literature by different methods (see for instance [21]). One of them consists to use a time-stepping or SIMPLE-like algorithm to decouple the pressure and velocity unknowns and then solve the pressure unknowns by a finite volume Laplacian operator which differ from the discrete divergence operator applied to the discrete gradient operator.

In this work, we have preferred to simultaneously solve the velocity and the pressure unknowns in order to preserve the accuracy of the scheme at the boundary of the domain. Therefore, an explicit stabilization method is introduced, following some ideas of [19] in the framework of the finite element method. Such a choice of stabilization would correspond to $\lambda_{KL}=\lambda h^\alpha$ for all pairs of neighboring control volumes, where λ is adjusted with respect to the studied problem, h is the maximal size of the control volumes and $\alpha\in[0,2]$ is an adjustable exponent. A drawback of this method is that it yields some redistribution of the fluid mass over the whole domain.

An original stabilization method has therefore been introduced. The family of control volumes $\mathcal{M}$ has been partitioned into disjoint subsets including groups of neighboring control volumes. The criterion to be respected is that the distance between two control volumes belonging to the same subset is bounded by Ch, where h is the maximum size of the control volumes and, C is about 2 or 3 for example. Then the stabilizing parameter λ_{KL} is chosen equal to λ for any pair of neighboring control volumes K and L belonging to the same subset, 0 otherwise. The value λ is a positive value, chosen large enough for preventing from the apparition of instabilities.

We have implemented the following algorithm for partitioning $\mathcal{M}$:

- select an order for the control volumes K_i, $i = 1, M$;
- for $i = 1$ to M, if K_i and all its neighbors do not yet belong to a subset, initialize a new one by K_i and all its neighbors;
- for $i = 1$ to M, if K_i does not yet belong to one of the subsets, one of its neighbor does: include K_i in this subset.

We shall present in a further paper the mathematical study of the convergence of this stabilized scheme. Note that a crucial difference with the stabilization of [19] is that there is no need to let λ tend to 0 with the size of the mesh, which means that the presence of a finite stabilization does not decrease the quality of the approximation. The numerical examples given below illustrate this kind of property.

2.6 Numerical implementation of the scheme

The schemes (4) or (5) resume to a set of linear and nonlinear equations under the following form: $\mathcal{E}_j\left([x_k]_{k=1,\mathcal{N}}\right) = 0$, for $j = 1, \mathcal{N}$, where $[x_k]_{k=1,\mathcal{N}}$ is the vector gathering in the transient case the components of $\vec{v}_K^{n+1/2}$, $p_K^{n+1/2}$ and $T_K^{n+1/2}$, for all $K \in \mathcal{M}$, and in the steady case the components of $\vec{v}_K$, p_K and T_K. For example, with M control volumes for a 3D thermal problem, then $\mathcal{N} = 5M$.

Newton's method consists in first selecting an initial guess $\left[x_k^{(0)}\right]_{k=1,\mathcal{N}}$ of $[x_k]_{k=1,\mathcal{N}}$, which we choose equal to the values given at the beginning of the time step for a transient problem. Then at the iteration l, the solution $\left[\delta x_j^{(l)}\right]_j$ of the following linear system

$$\left[\frac{\partial \mathcal{E}_i}{\partial x_j}\left(\left[x_k^{(l)}\right]_k\right)\right]_{i,j} \times \left[\delta x_j^{(l)}\right]_j = -\left[\mathcal{E}_i\left(\left[x_k^{(l)}\right]_k\right)\right]_i$$

is computed either by a direct solver or by an iterative one, BICGSTAB in our examples. The under-relaxation factor θ

$$\theta = \min\left(\frac{\delta_0}{\left\|\left[\delta x_j^{(l)}\right]_j\right\|}, 1\right)$$

is then calculated, taking for δ_0 a small enough value preventing from oscillations of the iterative method. Note that the quadratic convergence of Newton's method is preserved close

enough to the solution ($\left\| \left[\delta x_j^{(l)}\right]_j \right\| < \delta_0$), obviously as long as the linear systems are precisely solved. A new approximation of the nonlinear system is determined by the relation

$$\left[x_j^{(l+1)}\right]_j = \left[x_j^{(l)}\right]_j + \theta \left[\delta x_j^{(l)}\right]_j .$$

The iterations are stopped when $\left\| \left[\delta x_j^{(l)}\right]_j \right\|$ is lower than a given criterion (indeed much smaller than δ_0). It is worth to point out that the precision of the solver is only related to the Newton criterion, and not to the accuracy of the solution of the linear solver.

3 Numerical studies

Computations have been performed on a personal computer with a 3 GHz Pentium 4 processor with 1Go of memory.

3.1 Analytical test: the decaying vortices

We verify the temporal and spatial accuracy of this numerical scheme by simulating the solution

$$\begin{aligned} u(x,y,t) &= -\cos(\pi x) sin(\pi y) \exp(-2\pi^2 t/Re) \\ v(x,y,t) &= \sin(\pi x) cos(\pi y) \exp(-2\pi^2 t/Re) \\ p(x,y,t) &= -\frac{\cos(2\pi x) + cos(2\pi y)}{4} \exp(-4\pi^2 t/Re) \end{aligned}$$

on the square $[-0.5, 0.5] \times [-0.5, 0.5]$ domain, simply by imposing the above time dependent values of the velocity at the boundary of the domain and introducing its values at $t = 0$ as initial conditions in the domain. The computations were performed for $Re = 10$ using a regular square grid.

We use the direct linear solver for the meshes 40×40, 80×80 and 160×160 and the iterative solver BICGSTAB for the finest grid 320×320, keeping the time step constant at $\Delta t = 0.001$. The difference between the analytical and computed velocity is presented in figure 2(a), and shows the spatial second order accuracy of the scheme.

Next, by varying the time step and by keeping the mesh size constant, namely the finest grid 320×320, we study the temporal accuracy. Figure 2(b) presents the variation of the difference between the analytical and computed velocity and shows that the time integration scheme is second-order accurate too.

3.2 Closed isothermal cavity test cases

We consider in this section different lid-driven problems. The Reynolds number, Re, is based upon the imposed tangential velocity along the moving wall and the length of one side of the cavity.

2d-square cavity

Computations have been performed in the case of a 2d-square lid driven cavity with $Re = 1\,000$, using square meshes. Our results are compared with the numerical works of Botella and Peret [22] achieved with a spectral method (**SP**) using Chebyshev polynomials.

The values of the velocity extrema along the centerlines of the cavity and the values of the stream function at the square center (Tab. 1) are in excellent agreement with the benchmark reference. For the coarsest grid, the relative difference with the reference does not exceed 2%.

For the finest grid, the stabilizing and relaxation parameters are $\lambda = 10^{-7}$ and $\delta_0 = 100$, respectively. The computation time is about 26 minutes using the linear solver BICGSTAB with an ILU preconditioning based on 6 levels.

2d-inclined cavity

In the case of a 30° inclined driven cavity, we compare our results with Mathur and Murthy's ones, obtained on a 6 400 triangular finite volume cells (**FV**) for $Re = 1\,000$ [15]. Figures 3(a) and 3(b) illustrate, for a coarse Voronoï meshes, the hexagonal grid and the groups of neighboring control volumes used to stabilize the checkerboard pressure modes.

The horizontal and vertical components of the velocity at the centerlines, drawn in figure 4, are in agreement with those of [15] (the values of [15] have been scanned before plotting; since the range of the vertical component is small, the corresponding values of [15] are only imprecisely known, and a drawing at the same scale as u would lead to confounded curves). The minimum of the horizontal component of the velocity along the vertical centerline and its location are reported in Table 2 and are in agreement with [15].

For 29 737 cells, the computation parameters are $\lambda = 10^{-6}$ and $\delta_0 = 100$ for a CPU time of 2 minutes. The linear solver BICGSTAB is used with an ILU preconditioning based on 5 levels.

3d lid-driven cavity

The computational domain is the $[0,1] \times [0,1] \times [0,1]$-cube. A tangential velocity is imposed on the upper wall defined by $z = 1$. Computations have been performed on a nonuniform orthogonal $36 \times 36 \times 36$ grid refined at the boundaries: the side of the control volumes satisfies a geometric series with a ratio equal to 1.2.

The velocity profiles are successfully compared with the unstructured finite volume (**FV**) [23] and trilinear finite element (**FE**) [24] methods for $Re = 400$ and $Re = 3200$ (Fig. 5).

The extremum values of the velocity components as well as their location are summarized in Table 3. Most of the results are in agreement, except for the coordinate x corresponding to the maximal vertical component w of the velocity, with $Re = 3200$.

The stabilizing parameter is $\lambda = 10^{-5}$. The computation time is respectively about 7 and 80 minutes for $Re = 400$ and $Re = 3\,200$, using a 3-levels ILU preconditioning.

3.3 Open channel: the backward facing step

We consider the laminar flow of a Newtonian fluid over the 0.94 backward facing step in a channel of height 1.94. A Poiseuille velocity profile is prescribed at the inlet boundary and the value of the pressure is imposed at the outlet. Computations have been performed for Reynolds numbers up to $Re = 4HU_{max}/(3\nu) = 800$, with U_{max} the maximum Poiseuille velocity and H the height of the channel before the downward step ($H = 1$). We use a Voronoï mesh with 39 306 non-uniformly distributed cells (essentially of hexagonal shape). Figure 6(a) shows an enlargement of the grid in the vicinity of the backward facing step, whereas the groups of the neighboring control volumes are shown in Figure 6(b).

Table 4 reports the good agreement of the reattachment lengths of the first and the second vortices divided by the step height for $Re = 800$.

The stabilization and relaxation parameters are respectively equal to $\lambda = 10^{-4}$ and $\delta_0 = 100$ for a CPU time of 6 minutes for $Re = 800$. The linear solver BICGSTAB is used with an ILU preconditioning based on 5 levels.

3.4 Natural convection flow

We consider the two-dimensional natural convection flow in a square cavity filled with air ($Pr = 0.71$), differentially heated on its vertical walls and isolated on the others. Computations have been performed for $Ra \in [10^6, 10^8]$, on a nonuniform orthogonal grid, the side of the control volumes following a sinusoidal distribution. Results are compared with the benchmark solutions of Le Quéré [25] obtained with a pseudo-spectral Chebyschev method (**SP**).

Table 5 presents, for $Ra = 10^8$ and for different meshes, the values of velocity extrema along the centerlines of the cavity, the average Nusselt number at the hot wall and the stream function at the center of the cavity.

For the finest grid, the stabilization and relaxation parameters are respectively $\lambda = 10^{-6}$ and $\delta_0 = 100$ for a CPU time of 85 minutes. The linear solver BICGSTAB is used with an ILU preconditioning based on 2 levels.

4 Conclusion

Considering the above numerical examples, the properties shown on the new finite volume scheme presented in this paper confirm that it can be successfully used in a relatively wide range of test cases. Its implementation is quite simple, thanks to the fact that this scheme only involves simple geometric factors and is a natural finite volume scheme, such that all the differential operators have been approximated at the interfaces between control volumes. An upstream version of the interface terms could be used in the case of coarse meshes, permitting that this scheme be used in an industrial framework. The accuracy of the results on classical tests of the literature is correct for small or acceptable computing times, even in one 3D case. The question of the use of this scheme on larger meshes then arises. Indeed, its computational cost seems to be higher than that of a pressure-corrector based method, since it leads to linear systems coupling all the unknowns. Let us observe that a pressure-corrector based method,

applied to the steady linear Stokes problem, can be viewed as an iterative method, belonging to the class of Gauss-Seidel methods. The rate of convergence of such a method is then linear. Hence, the scheme that we study in this paper uses Newton's method, which is a fixed point method with a quadratic rate of convergence. All the computing performances are then linked with the linear solver which is used. Since the structure of the coupled linear systems is similar to that of the initial Stokes problem, a pressure-corrector based method could then be used as a preconditioner. We have preferred here to use a preconditioner based on an incomplete factorization, in order to be able to enforce, if needed, the robustness of the iterative method.

So we expect that our further works will confirm this analysis, and that it will be possible to handle larger problems, by developing faster preconditioners (a way will be to use libraries of linear solvers dedicated to parallel computers). Another direction of research is the determination of an optimal coupling between the precision of the nonlinear resolution and that of the linear systems. Let us finally mention that we are actually developing a version of the scheme for the Navier-Stokes equations without using Boussinesq's approximation, and for weakly compressible problems. We have already obtained encouraging results.

References

1. D. Kwak, C. Kiris and C.S. Kim, Computational Challenges of Viscous Incompressible Flows, *Computers and Fluids*, vol. 34, pp. 283-299, 2005.

2. V. Girault and P.A. Raviart, *Finite Element Methods for the Navier-Stokes Equations: Theory and Algorithms*, Springer, Berlin, 1986.

3. O. Pironneau, *Finite Element Methods for Fluids*, Wiley and Sons, 1989.

4. M.D. Gunzburger, *Finite Element Methods for Viscous Incompressible Flows, A Guide to Theory, Practice, and Algorithms*, Academic Press, 1989.

5. R. Glowinski, Numerical Methods for Fluids (Part3), *Handbook of Numerical Analysis*, P.G. Ciarlet and J.L. Lions (Eds.), vol. 9, 2003.

6. S.V Patankar, *Numerical Heat Transfer and Fluid Flow*, MacGraw-Hill, New-York, 1980.

7. F. Harlow and J. Welch, Numerical Calculation of Time-Dependent Viscous Incompressible Flow of Fluid with a Free Surface, *Phys. Fluids*, vol. 8, pp. 2182-2189, 1965.

8. R.A. Nicolaides, The Covolume Approach to Computing Incompressible flows, M.D Gunzburger and R.A. Nicolaides (Eds.), *Incompressible Computational Fluid Dynamics*,pp. 295-333, Cambridge Univ.Press, Cambridge, U.K, 1993.

9. D. Vidovic, A. Segaland and P. Wesseling, A Superlinearly Convergent Finite Volume Method for the Incompressible Navier-Stokes Equations on Staggered Unstructured Grids, *J. Comput. Phys*, vol. 198, pp. 159-177, 2004.

10. R. Eymard and R. Herbin, A Cell-Centered Finite Volume Scheme on General Meshes for the Stokes Equations in Two Space Dimensions, *C. R. Math. Acad. Sci. Paris*, vol. 337(2), pp. 125-128, 2003.

11. P. Blanc, R. Eymard and R. Herbin, A Staggered Finite Volume Scheme on General Meshes for the Generalized Stokes problem in two space dimensions, *Int. J. on Finite Volumes*, http://averoes.math.univ-paris13.fr/JOURNAL/IJFV/, 2005.

12. R. Eymard and R. Herbin, A staggered finite volume scheme on general meshes for the Navier-Stokes equations in two space dimensions, *Int. J. on Finite Volumes*, http://averoes.math.univ-paris13.fr/JOURNAL/IJFV/, 2005.

13. C.M. Rhie and W.L. Chow, Numerical Study of the Turbulent Flow Past an Airfoil with Trailing Edge Separation, *AIAA J.*, vol. 21, pp. 1523-1532, 1983.

14. S.R. Mathur and J.Y Murthy, A Pressure-Based Method for Unstructured Meshes, *Numer. Heat Transfer*, vol. 31, pp. 195-215, 1997.

15. S.R. Mathur and J.Y Murthy, Pressure Boundary Conditions for Incompressible Flow Using Unstructured Meshes, *Numer. Heat Transfer*, vol. 32, pp. 283-298, 1997.

16. L. Davidson, A Pressure Correction Method for Unstructured Meshes with Arbitrary Control Volumes, *Int. J. Numer. Meth. Fluids*, vol. 22, pp. 265-281,1996.

17. S. Perron, S. Boivin and J.M Hérard, A Finite Volume Method to Solve 3D Navier-Stokes Equations on Unstructured Collocated Meshes, *Computers and Fluids*, vol. 33, pp 1305-1333, 2004.

18. A.J. Chorin, Numerical Solution of the Navier-Stokes Equations, *Math. Comput.*, vol. 22, pp. 745-762, 1968.

19. F. Brezzi and J. Pitkaranta, On the Stabilization of Finite Element Approximations of the Stokes Equations, *Notes Numer. Fluid Mech., Vieweg, Braunschweig*, vol. 10, 1984.

20. R. Eymard, R. Herbin and J.C Latché, Colocated Finite Volume Scheme on General Meshes for the Incompressible Navier-Stokes Problem in Two or Three space, *SIAM J. on Numer. Analysis, submitted.*

21. A.W. Date, Fluid Dynamical View of Pressure Checkerboarding Problem and Smoothing Pressure Correction on Meshes with Colocated Variables, *Int. J. Heat and Mass Transfer*, vol. 46, pp. 4885-4898, 2003.

22. O. Botella and R. Peyret, Benchmark Spectral Results on the Lid-Driven Cavity Flow, *Computers and Fluids*, vol. 27(4), pp. 421-433, 1998.

23. C.H. Tai, Y.Zhao and K.M Liew, Parallel Computation of Unsteady Three-Dimensional Incompressible Viscous Flow Using an Unstructured Multigrid

Method, *Computers and Structures*, vol. 82, pp. 2425-2436, 2004.

24. Bo-nan Jiang, T.L. Lin and L.A. Povinelli, Large Scale Computation of Incompressible Viscous Flow by Least-Square Finite Element Method, *Comput. Meth. Appl. Mech. Eng.*, vol. 114, pp. 213-231, 1994.

25. P. Le Quéré, Accurate Solutions to the Square Thermally Driven Cavity at High Rayleigh Number, *Computers and Fluids*, vol. 20(1), pp. 29-41, 1991.

26. B.F. Armaly, F. Durst, J.C.F. Pereira and B. Schönung, Experimental and Theoretical Investigation of Backward-Facing Step Flow, *J. Fluid Mech.*, vol. 127, pp. 473-496, 1983.

27. T.P. Chiang, TONY W.H. Sheu and S.F. Tsai, Topological Flow Structures in Backward-Facing Step Channels, *Computers and Fluids.*, vol. 26, pp. 321-337, 1997.

28. J. Kim and P. Moin, Application of a Fractionnal-Step Method to Incompressible Navier-Stokes Equations, *J. Comput Phys.*, vol. 59, pp. 308-323, 1985.

29. L. Kaiktsis and G.E.M Karniadakis and S.A Orszag, Onset of Three-Dimensionality, Equilibria, and Early Transition in Flow over a Backward-Facing Step, *J. Fluid Mech.*, vol. 231, pp. 501-528, 1991.

Table 1: Lid driven cavity, $Re = 1000$

nx×ny	80×80	150×150	220×220	**[22]** (96×96, **SP**)
$u_{max}(0.5, y)$	0.3813 (1.9%)	0.3870 (0.4%)	0.3877 (0.2%)	0.3886
y	0.175 (1.9%)	0.173333 (0.9%)	0.172727 (0.5%)	0.171785
$v_{max}(x, 0.5)$	0.37125 (1.5%)	0.37543 (0.4%)	0.37607 (0.2%)	0.37695
x	0.844 (0.2%)	0.8433 (0.1%)	0.8432 (0.1%)	0.8422
$v_{min}(x, 0.5)$	-0.5205 (1.3%)	-0.5251 (0.4%)	-0.5260 (0.2%)	-0.5271
x	0.09 (0.8%)	0.09 (0.8%)	0.0909 (0.1%)	0.0908
$\psi(0.5, 0.5)$	0.11705 (1.6%)	0.11801 (0.7%)	0.11867 (0.2%)	0.11893

Table 2: Inclined lid driven cavity, $Re = 1\,000$

	Present work			[15]
Number of cells	5 643	14 040	29 737	6 400, **FV**
$u_{min}(0.5, y)$	-0.194	-0.197 (1.6%)	-0.197 (1.6%)	-0.194 (1.6%)
y	0.78	0.78	0.78	0.78

Table 3: The values of the velocity extrema $u(0.5, 05, z)$ and $w(x, 0.5, 0.5)$ for $Re = 400$ and $Re = 3200$

	$Re = 400$			$Re = 3200$	
	Present work	[23], **FV**	[24], **FE**	Present work	[23], **FV**
	46 656 cells	24 389 nodes	$50 \times 52 \times 50$		97 336 nodes
$u_{min}(0.5, 05, z)$	-0.221 (1.4%, 7%)	-0.218	-0.238	-0.286 (0.85%)	-0.285
z	0.229 (0.9%, 11%)	0.227	0.257	0.06	0.06
$w_{max}(x, 0.5, 0.5)$	0.20 (5%)	0.187		0.230 (5%)	0.214
x	0.15	0.15		0.0626 (20%)	0.050
$w_{min}(x, 0.5, 0.5)$	-0.37 (3%)	-0.360		0.428 (3%)	0.415
x	0.87 (1.2%)	0.86		0.95	0.95

Table 4: Reattachement lengths, $Re = 800$

	1st vortex (x/s)	2nd vortex (x/s)
Armaly *et al.* (experimental results) [26]	14.2	20.0
Chiang *et al.* [27]	12.3	20.8
Kim & Moin [28]	12.0	
Kaiktsis *et al.* [29]	11.9	
Present work	12.2	20.1

Table 5: Natural convection, $Ra = 10^8$

	Present work			**[25]**
	100×100	200×200	300×300	128×128, **SP**
Solver	direct	direct	iterative	
$u_{max}(0.5, y)$	300.525 (6.7%)	313.677 (2.5%)	317.463 (1.4%)	321.876
y	0.930 (0.22%)	0.930 (0.22%)	0.925 (0.33%)	0.928
$v_{max}(x, 0.5)$	2200.95 (0.9%)	2215.67 (0.3%)	2218.47 (0.17%)	2222.39
x	0.012	0.012	0.012	0.012
$\Psi(0.5, 0.5)$	52.37 (0.1%)	52.34 (0.04%)	52.33 (0.02%)	52.317
$\overline{Nu}$	30.232 (0.07%)	30.228 (0.06%)	30.210 (0.03%)	30.209

List of Figures

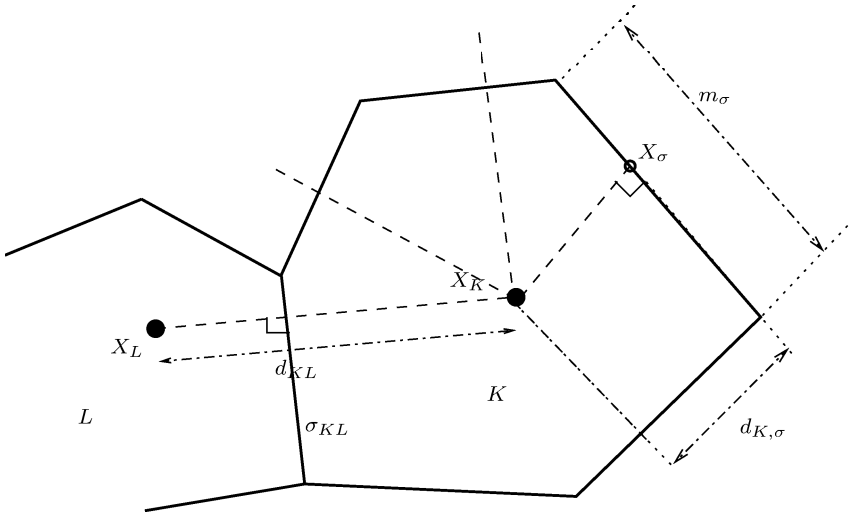

Figure 1: Control volume and geometry definitions

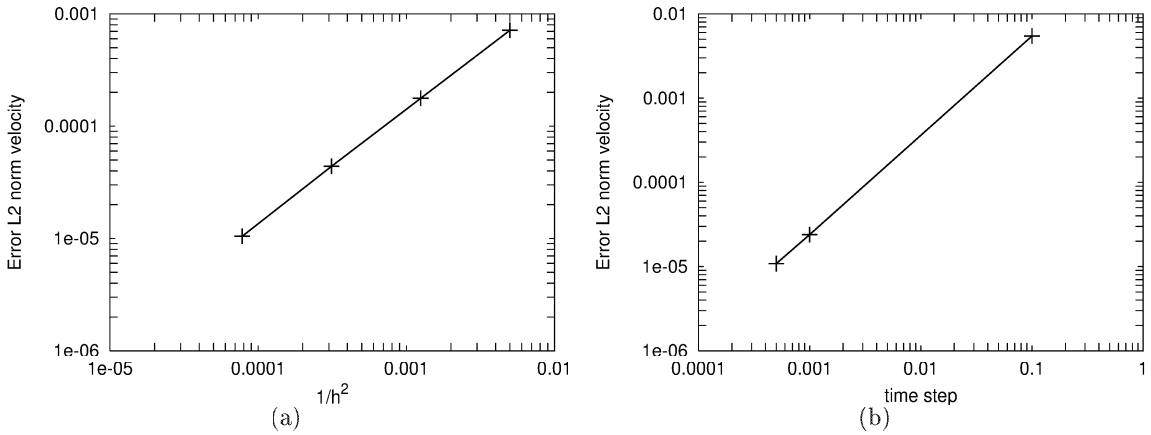

Figure 2: Convergence rate in time and space

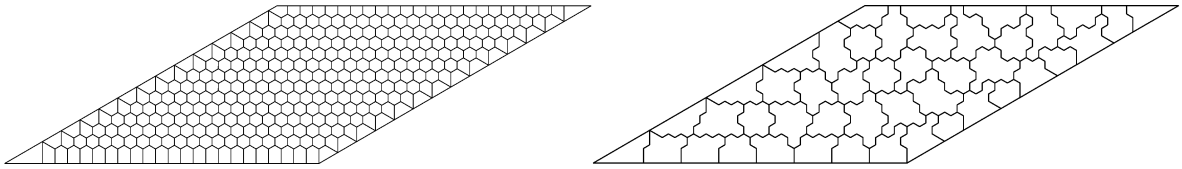

(a) (b)

Figure 3: Voronoï mesh and groups of neighboring control volumes

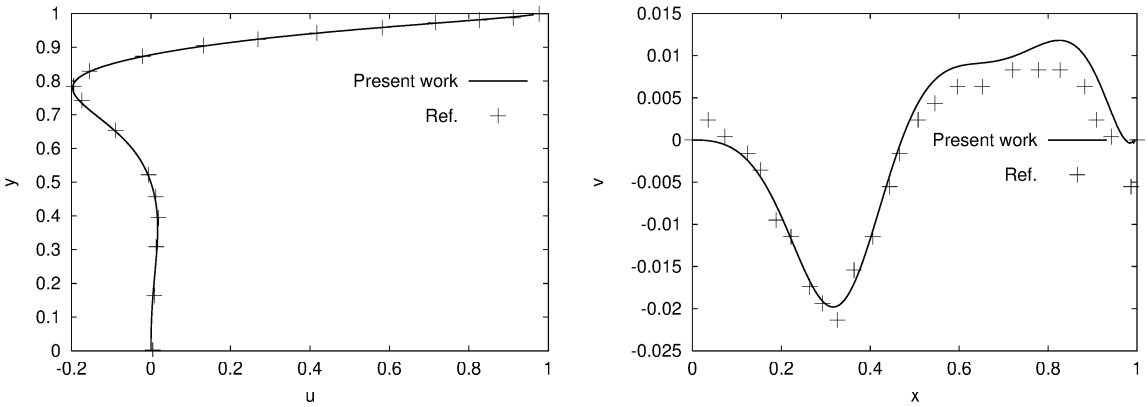

(a) (b)

Figure 4: Profile of horizontal and vertical velocity components at the centerlines for $Re = 1000$

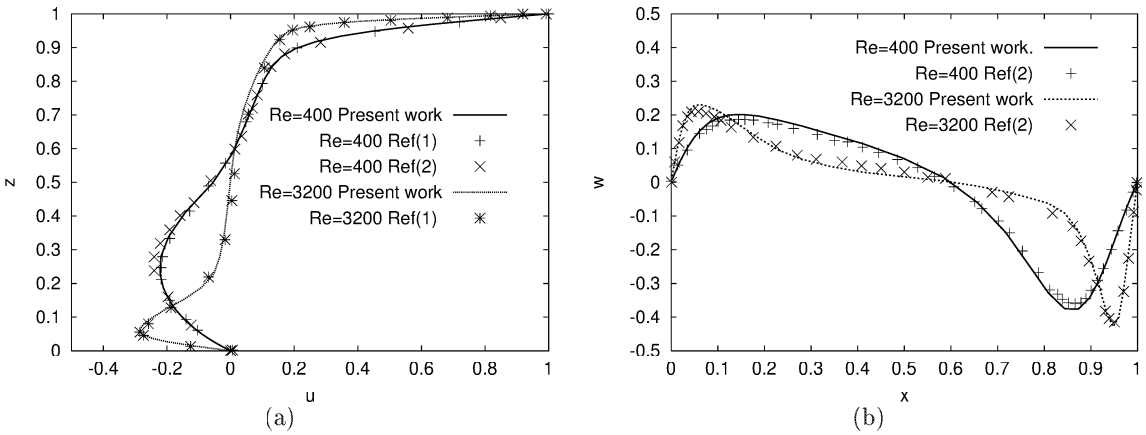

(a) (b)

Figure 5: 3d Lid-driven cavity flow, comparisons with Ref(1) ([24]) and Ref(2) ([23]).

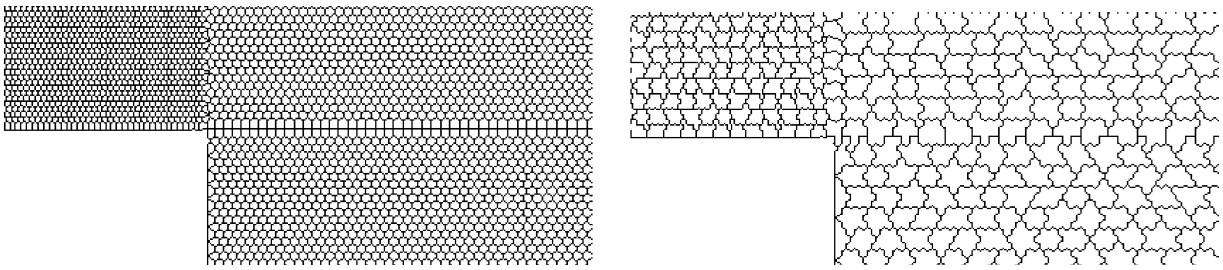

(a) (b)

Figure 6: Voronoï mesh and groups of neighboring control volumes.